Egypt. J. Chem. **Vol. 67,** No. 6 pp. 445 - 456 (2024)

Egyptian Journal of Chemistry

http://ejchem.journals.ekb.eg/

Rapid RP-HPLC Detection Method For Quantification Of Gentamicin Sulfate Loaded Wound Dressing Nanofiber Formulation With Accelerated In Vivo Wound Healing

Mona M. Agwa [1*], Mohamed R. El-Aassar [2,3*], Rehab I. Moustafa[4], Hassan Elsayed [4] , Nagham G. El-Beheri [3].

[1]*Department of Chemistry of Natural and Microbial Products, Pharmaceutical and Drug Industries Research Institute, National Research Centre, Dokki, Giza, 12622, Egypt.*

[2]*Department of Chemistry, College of Science, Jouf University, Sakaka 2014, Saudi Arabia.*

[3]*Polymer Materials Research Department, Advanced Technology and New Materials Institute, City of Scientific Research and Technological Applications (SRTA-City), New Borg El-Arab City, Universities and Research Institutes District, Alexandria 21934, Egypt.*

[4]*Department of Microbial Biotechnology, Biotechnology Research Institute, National Research Centre, Dokki, Giza 12622, Egypt.*

Abstract

Wound healing is a complex and dynamic procedure which demands a proper climate to reinforce quick remedy. Gentamicin is a broad spectrum amino glycoside antibiotic having a potent bactericidal impact, but its implication is restricted by the minimal bioavailability, shortened half-life, and nephrotoxicity. In this work, a controlled release gentamicin sulfate formulation was constructed employing PGA-HA/PVA wound dressing nanofiber. The loss of UV chromophores in gentamicin structure restrains a straightforward emergence of analytical method. In this context, a validated reversed-phase high-performance liquid chromatography method for the rapid quantification of gentamicin sulfate content in the nanofiber delivery system was eveloped. The nanofibrous scaffold were constructed from hyaluronic acid, polyvinyl alcohol, and Polygalacturonic acid for accelerating wound healing. The morphology of nanofibers were checked by SEM. The mean diameter of the nanofibers were 360 nm. The FT-IR characterizations disclosed the incorporation of gentamicin into the nanofibers. The presence of gentamicin induces changes in the mechanical properties via influencing the material's ability to withstand tensile forces and deformation. In vivo wound healing on the wistar rats disclosed a faster healing for animals treated with PGA-GM-HA/PVA nanofiber that confirmed by histopathological examination compared to those applied sterile gauze.

Keywords: RP-HPLC, Wound dressing nanofiber; Gentamicin; Sterile gauze; Electrospinning; Polygalacturonic acid; and Hyaluronic acid.

1. Introduction

Wound healing is a complex and dynamic procedure which demands a proper climate to reinforce quick remedy. The mechanism of healing is a multistage technique and involves integration of successive and overlapping phases namely homeostasis, inflammation, proliferation and tissue remodeling. Unfortunately, the pathogenic bacteria and their toxins can pass deeply to various tissues by blood following attachment to the exposed wound area causing severe toxicity[1]. Gentamicin (GM) is mainly created by *Micromonospora purpurea* fermentation. It is categorized as broad spectrum amino glycoside antibiotic having a potent bactericidal impact towards both Gram-positive and Gram-negative pathogens when integrated into pharmaceutical dosage forms as an active ingredient[2]. Some antibiotics like gentamicin displayed other biochemical actions than fighting pathogens involving anti-inflammatory effect[3]. Some studies indicated that the anti-inflammatory action was attributed to the creation of superoxide by neutrophils subjected to stimulating agents while other proved that the antibiotic manifested an anti-inflammatory activity owing to suppressing of neutrophil NADPH oxidase stimulation[4, 5]. Although all these merits, the utilization of gentamicin powder is restricted by the minimal bioavailability, short half life, and may provoke adverse effects involving nephrotoxicity and ototoxicity. Thus, construction of a sustained release gentamicin dosage form employing natural polymers is urgently demanded and may have clinical profits[6].

Gentamicin sulfate (GMS) have been formerly investigated in multiple of nano-delivery systems [7] involving caroboxymethyldextran-b-poly(ethyleneglycols)[8], chitosan[9], poly(lactide-co-glycolide) (PLGA)[10], mesoporous silica[11], and gold nanoparticles[12]. A novel wound dressing electrospun nanofibrous scaffolds incorporating GMS have been previously fabricated via electrospinning technique for accelerated wound healing[13, 14].

Electrospinning is a technique that employs natural and synthetic polymers for the generation of nanofibrous (NFs) mats correspondence to the extracellular matrix having preferable mechanical strength, good absorption of wound

*Corresponding author e-mail: magwa79@gmail.com.; mona.m.agwa@alexu.edu.eg; mohamedelaassar@gmail.com

Receive Date: 02 December 2023, Revise Date: 20 January 2024, Accept Date: 21 January 2024

DOI: 10.21608/EJCHEM.2024.252585.8939

fluids ,considerable flexibility in surface functionalization, and an interconnected porous construction for nutrient and oxygen breakthrough[15]. Additionally, NFs could be employed as carriers to construct wound dressing for targeted and controlled delivery of active therapeutics in skin disorder[16]. Both natural or synthetic polymers are utilized in the fabrication of NFs [17]. The majority of the biocompatible and biodegradable natural polymers employed in the construction of NFs involving hyaluronic acid, gelatin, chitosan, silk fibroin, chondroitin sulfate, and collagen are beneficial for biomedical purposes. However, they exhibited a limited solubility in organic solvents, high surface tension, and poor mechanical properties, which render it more complicated to construct NFs from natural polymers[18]. Some synthetic biocompatible and biodegradable polymers involving poly vinyl alcohol (PVA), Polycaprolactone, and Polyglycolic acid (PGA) could be integrated with natural polymers during NFs fabrication to mend the mechanical properties[19].

Hyaluronic acid (HA) deemed one of the preferable natural Polysaccharide employed for wound healing handling, owing to its biocompatibility, non-immunogenicity, biodegradability, anionic nature, and atypical physicochemical qualities. It is highly hydrophilic; therefore, it has a powerful function in removing lots of wound exudates[20]. Additionally, it exerts a remarkable role in supporting cells through the healing stages via collagen deposition and angiogenesis[21, 22] The proceeding in electrospinning methods integrated both novel natural biomaterials and therapies commanded the advancement of NFs from passive protective wound covers to bioactive/interactive reinforcing cell regeneration biomaterial[23]. Incorporating NFs with antibiotics has been reported to improve vascular and cellular propagation, thus hastening the cutaneous lesions closure, as well as being efficacious in diminishing infection[24].

Chromatographic method particularly high-performance liquid chromatography deemed to be applied primarily for the quantitative assessment of aminoglycosides. Owing to their elevated polarity, minimal solubility in organic solvent, high water solubility, nonvolatility, and the lacking of powerful UV absorbing chromophore, the quantitative assessment of aminoglycosides GMS in pharmaceutical formulations demand derivatization, , and/ or specialized detectors for ameliorating their chromatographic performance[25, 26]. Derivatization methods with o-Phthalaldehyde (OPA) have the advantage of minimizing analysis time that takes place at room temperature but this derivatization process have lacking the stability of the solution and consequently affect the precision of the method[27]. Other detection methods involving Evaporative Light Scattering Detection (ELSD), and Refractive Index (RI) Detection have considerable obstacles and restrictions for harnessing in the routine GMS analysis[28]. The ELSD method is lacking the sensitivity and precision with narrow linear dynamic range, making it inappropriate for this analysis. On the other hand, RI method is inconsistent with the gradient mode which are substantial to detach the related materials of gentamicin[2]. Although mass spectrometry techniques (LC/MS) allow aminoglycosides detection, they are not vastly obtainable and demand well qualified trained operators[29].Thus, developing a simple RP-HPLC method to assess GMS in pharmaceutical dosage form using direct UV detection is needed. In all applied analysis cases including LC/MS methods, the utilization of fluorinated ion-pairing reagents involving pentafluoropropanoic acid (PFPA), trifluoroacetic acid (TFA), or heptafluorobutyric acid (HFBA) is essential[26]. Supplementing the mobile phase with ion-pairing agents upgrades retention, sensitivity, peak shape, and resolution of aminoglycosides and switches the RP separation mode to ion-pair RP liquid chromatography[30].

Herein, we report for the first time an optimized and validated fast and simple RP-HPLC-photo diode array (PDA) method using direct UV detection which allow the quantification of aminoglycosides, specifically GMS integrated HA based wound dressing nanofiber using formic acid (FA) as ion-pairing reagent. FA is often utilized with LC/MS detection as it doesn't cause ion suppression like TFA[31]. Other previous studies reported loading of gentamicin as antimicrobial agent into injectable thermo-sensible, HA based hydrogel[32, 33], polymeric blends based on collagen, chitosan and hyaluronic acid in the form of thin films[34], and binary collagen/hyaluronic acid membrane[35]. But up to our knowledge, no previous study reported loading of Gentamicin into hyaluronic acid based nanofiber. The manufactured drug loaded nanofiber are characterized using SEM (scanning electron microscope), thermal degradation, tensile strength, FTIR (Fourier-transform infrared spectroscopy), and water contact angle. The validated method was conducted to assess the drug loading and the in vitro release % into phosphate- buffered solutions. Additionally, the wound healing efficiency of GMS integrated nanofiber was examined in vivo regarding the % wound closure and histopathological examination.

2. Experimental

2.1. Materials

Gentamicin sulfate (GMS) with 99% purity were from Sigma-Aldrich (St Louis, MO, USA). PGA (Japan, Tokyo) was from TCI Chemicals. HA and PVA (Schnelldorf, Germany) were from Sigma-Aldrich. HPLC grade ACN (Acetonitrile), (99%), methanol (99.0%), Ethanol (99.0%), and Formic acid (99.5%) were from Fisher Scientific Co. (UK). Potassium dihydrogen phosphate (98.0%), sodium chloride (99.0%), disodium hydrogen phosphate (99.0%) were from Sigma Aldrich. Other utilized chemicals and reagents were of analytical grade.

2.2. Preparation of nanofiber incorporating gentamicin sulfate

1% (w/v) Polygalacturonic acid (PGA) aqueous solution was equipped at alkaline media and magnetic stirring for 0.5 h at ambient temperature followed by addition of 3% (w/v) gentamicin sulfate (GMS) and left for another 1 h under stirring till complete homogenization. The prepared solution of (0.25%w/v) HA was added to the formulated PGA-GM mixture under stirring at 50 °C for 1 h until complete homogenization followed by freeze drying. The spinnable liquid was constructed via mixing 8% PVA with 1% PGA-GM-HA/PVA under stirring till complete homogenization.

The constructed spinnable solution was introduced into glass syringe holding metalic capillary needle (0.5 mm diameter). "The electrospinning order (nanoNC needle laboratory instrument, Model: ESR100D, Seoul, Korea)" inclosed syringe pump & collector wrapped with aluminum foil, and high voltage power supply that transported to the

blend solution (PGA-GM-HA/PVA) in a syringe thru an alligator clasp agglutinated to the needle utilizing high voltage at 11 kV. The working polymer solutions were pushed out of the syringe pump at 1.3 ml/h feed rate. The space among the collector and the needle end was 17 cm. The constructed NFs were collected and allow to dry in an oven at 40°C under vacuum for 2 days. Dry NFs were assemble immediately from the collector and kept at desiccator[36, 37].

2.3. Characterization of the fabricated nanofiber

2.3.1. Scanning electron microscopy (SEM)

The morphological appearance of the constructed NFs (PGA-GM-HA/PVA & PGA-HA/PVA) were imaged by SEM (SEM, JSM-6360, JEOL, LLA, Japan). NF pieces were wrapped with gold and checked at an accelerating voltage (10 kV). The mean NFs diameter (n = 100) was estimated by "ImageJ" software version 1.6.0_20. The calculation were based on haphazardly nominated 100 NFs from the SEM picture.

2.3.2. Fourier transform infrared (FTIR) and Raman spectroscopy

FT-IR (Shimadzu FTIR-8400 S, Kyoto, Japan) was employed to resolve constituents and chemical construction of the PGA-HA/PVA and PGA-GM-HA/PVA NFs. The NFs were checked at a wavelength scope of 4000–400 cm^{-1} to define the present functional groups.

2.3.3. Thermogravimetric analysis (TGA)

The PGA-HA/PVA and PGA-GM-HA/PVA NFs thermal disintegration distinctive were emphasized using a Thermal Gravimetric Analyser (TGA-50, Shimadzu, Japan). This test was fulfilled in a nitrogen medium, applying a thermal average of 10 °C min^{-1} until attaining a temperature of 600 °C.

2.3.4. Tensile strength

The mechanical features of the PGA-HA/PVA and PGA-GM-HA/PVA NFs were assessed using a Shidmadzu model AG-I tensile testing instrument from Japan. NFs measuring 6mm in length and 1mm in width were checked at a crosshead speed of 30mm per minute. The NFs thickness was mounted with a precision of 0.001mm via a digital micrometer (Mituto, Japan, Tokyo). The average of five successive measurements was enumerated to attain the thickness value.

2.3.5. Water contact angle

The static contact angle (θ) of PGA-HA/PVA and PGA-GM-HA/PVA NFs were assessed via a (Ramé-Hart Device Goniometer, pattern 500-F1, France). This encompassed pouring water on the NFs at three distinct sites for measurement.

2.4. HPLC method assay for quantification of gentamicin sulfate

2.4.1. Equipment

HPLC-PDA analysis was implement utilizing a Shimadzu ProminenceLC-20AP equipped with an autosamplerSIL-10AP, communication bus module CBM-20A, quaternary pump LC-20AP, vacum degasser, and photodiode array detector (PDAD) SPD-20A. The reversed-phase proceeding harnessed an Inertsil ODS-3 (250 × 4.6 mm, 5 µm) column (GL Sciences, Torrance, USA). The monitoring of the HPLC system, attained and processed data series was by Lab Solutions software.

2.4.2. Chromatographic events

Chromatographic condition was implemented in an isocratic style. The mobile phase involved a blend of Acetonitrile and milliQ water acidified with formic acid (20: 80, v/v; pH 3.0 ±0.2) at an ambient surrounding temperature (25 ºC ±0.2). The injection volume was 30 µl at 2.0 ml/min flow rate for 18 min. All trials were adjusted at 280, and 212 nm as they are the preferable λ_{max} which supply the higher sensitivity required for GMS detection in the released specimens from the NFs.

2.4.3. Elaboration of both standard and sample GMS solutions

The main standard solution of GMS (10 mg%) was accomplished by dissolving 10 mg GMS in milliQ water (50 ml), then supplement with 50 ml PBS (phosphate buffer saline, pH 7.4) into a volumetric flask (100 ml). The calibration curve was made by diluting the original standard solution to 1, 2, 3, 4, 5, 6, 7, 8 and 9 mg%. They were prepared in triplicate by blending certain volume of stock GMS solution in 10 ml measuring flask with 1: 1v/v PBS / milliQ water to evaluate the calibration curve, linearity, LOQ (limit of quantification), and LOD (limit of detection). Three other concentration (2, 6 and 9 mg%) were made in triplicate to assess the accuracy & precision.

2.4.4. Method optimization and validation

The validation was implemented according to the ICH regulation (International Conference on Harmonization of Technical Requirements for Registration of Pharmaceuticals for Human Use)[38]. To certify the suggested analytical procedure, the linearity, precision, accuracy, recovery, LOD and LOQ were spotted.

Linearity was assessed by building a calibration curve employing mean peak areas against recognized dose of GMS (1, 2, 3, 4, 5, 6, 7, 8 and 9 mg%). The outcoming regression equation was employed to estimate the anonymous drug amount. The accuracy and precision tests were done employing lower, middle and higher concentration solutions. Accuracy is the proportion of the analyte attained by screening of a recognized dose of the drug. It was assessed by estimating the % recovery of the mean from 3 various concentration covering the entire linearity range involving 2, 6 and 9 mg% made in triplicate [38-40]. The proportion of SD (standard deviation) was calculated on 3 separate days (n = 3). These solutions were also utilized to assess the precision. Precision is the grade of repetition of the newly developed method that was estimated from the inter-day and intra-day, then registered as RSD% (Relative Standard Deviation) for a statistically significant number of triplicate amounts[40, 41]. The RSD% was gained by dividing the SE (standard error) (n = 9) by the evaluated amount multiplied by 100.

The LOD and LOQ are recognized as the least drug amount in the examined specimen that can be assessed by specific method under particular conditions. The LOQ is the least drug amount that can be detected with agreeable accuracy & precision[42]. Both LOD and LOQ were mathematically assessed according to ICH regulations via employing the relevance among the least dose in the calibration curve (C)

and its signal to noise ratio (S/N) [43] via applying the following equation:

$$\boldsymbol{LOD = C \times 3/(S/N),\quad LOQ = C \times 10/(S/N)}$$

2.4.5. Determination of encapsulation efficiency (%EE)

For determination of GMS encapsulation efficiency (EE) in the NFs, a particular weight (10mg) of the NFs loaded GMS was disintegrated in milliQ water under sonication for 0.25 h (using UC, 10-250H, new lab, USA sonicator) to release the loaded GMS which then detected by the validated method (title 2.4.2.). The % entrapped GMS was quantified by dividing the amount of the GMS found in NFs by the overall amount of the GMS submitted during the preparation [1, 44, 45].

$$\%\boldsymbol{EE} = \frac{\boldsymbol{Mass\ of drugs\ in\ nanoparticles}}{\boldsymbol{Mass\ of\ drugs\ used\ in\ formulation}} \times \mathbf{100}$$

2.4.6. *In vitro* GMS Release

The *in vitro* GMS release from the constructed NFs and free GMS solution was checked employing dialysis bag method. NFs incorporating 5 mg GMS were inserted into dialysis bags (12–14 kDa MWCO VISKING dialysis, SERVA, Germany). The bags were inserted into 10 ml of PBS (pH 7.4; 37 °C) under shaking (100 rpm) to keep sink conditions. At planned time periods, 1 ml of the release medium were dragged followed by decompensation with the corresponding dragged amount of fresh release medium[36, 46]. All specimens were run in triplicates, and the dose of the liberated GMS was quantified by the new method (title 2.4.2.).

2.5. *In vivo* wound healing assessment

The rats underwent this experiment were 10 adult Wister male (8 weeks old), each weighting nearly 185–200 g. All steps were conducted according to the Institutional Animal Care and Use Committee at Alexandria University (ALEXU-IACUC-14/190806-3-1). Each rat was homed alone in an independent cage, with free access to standard diet and mineralized water ad libitum. The wound surgery was execute following our former published data to create deep, full-thickness rounded wounds, with a diameter of about 15 mm [47-49]. The wounded animals were sectioned into douple groups each involving five animals. For the first one (control group), the wounds were enveloped with sterile gauzes, while the wounds of the second group were treated by the manufactured PGA-GM-HA/PVA wound dressings NFs equivalent to 4mg GMs and covered with sterile gauze. Finally, wounds in both groups were secured in their sites by overlaying them with medical plaster tapes. During the duration of the trial, that expanded for 14 days, the wounds were checked at various durations, and their morphometric manifestations were recorded employing a digital camera. The % shrinkage of every wound was registered and compared to that of the starting wound. The % of wound shrinkage was quantified via the following equation [37, 50].

$$\boldsymbol{Wound\ shrinkage}\ (\%) = \mathbf{1} - \frac{\boldsymbol{Wound\ area\ at\ the\ given\ day}}{\boldsymbol{wound\ area\ at\ the\ day\ zero}}\ \mathbf{X\ 100}$$

At the terminus of every examination procedure, all the utilized sterile gauzes and PGA-GM-HA/PVA wound dressings NFs, were substituted by fresh clean ones. Also, the histopathological checking of the skins was execute employing one animal from every group on the 14th day via staining the skin with H&E (Haematoxylin and Eosin) or MTs (Masson's trichrome) stains. The former staining method was employed to specify the elemental skin structures that reside the dermal layer involving the blood vessels, hair follicles, and sebaceous glands, while the other second sort was employed for the extra monitoring of collagen deposition quality at the epidermis [51, 52]. The prepared sections at 100× magnification power were checked employing Polarized optical microscope (Leica Microsystems, Leica DM750P, Switzerland, Ltd).

2.6. Statistical analysis

Statistical analysis was performed using Graphpad prism version 9. The collected data were statistically analyzed using the mean and standard deviation M ± SD.

3. Results and discussion

3.1. Characterization of the constructed Nanofibers

3.1.1. Morphological characteristics of nanofibers structure

The surface characteristics and dimensions of PGA-HA/PVA and PGA-GM-HA/PVA NFs were checked using scanning electron microscopy (SEM). As depicted in Figure 1a and b, the PVA/PGA-HA NFs display an estimated diameter of 221 nm, whereas the PVA/PGA-HA-GM nanofibers exhibit diameters of 360 nm. A comparison between the average diameters of the two types of nanofibers reveals a 61% increase in diameter for the PVA/PGA-HA-GM variant. This augmentation may be attributed to the incorporation of gentamicin in the PVA/PGA-HA solution, resulting in heightened electrical charges on the liquid droplet's surface[53]. Despite this, no significant alterations in the morphology of the nanofibers were observed.

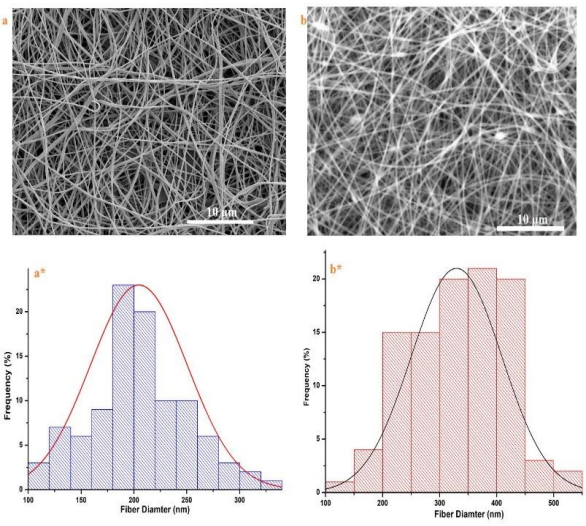

Figure 1: SEM images and particle size analysis of (a). PGA-HA/PVA, and (b). PGA-GM-HA/PVA NFs

3.1.2. FTIR analysis

FTIR spectra were utilized to detect distinctive peaks and significant alterations occurring in the polymer blend and

gentamicin loading. In Figure 2, the infrared absorption spectrum of PGA-HA/PVA NFs were checked both with and without GMS, notable shifts and changes in peak positions can be observed. The addition of GMS induces discernible modifications in the characteristic peaks associated with various functional groups present in the polymer. Specifically, in the infrared absorption spectra of PGA-HA/PVA NFs with GMS, shifts in the stretching peaks of O-H and N-H are evident, typically observed from approximately 3442 cm^{-1} to 3532 cm^{-1} [54]. Moreover, alterations are noticed in the C–H stretching from around 2935 cm^{-1} to 2941 cm^{-1}, along with changes in the C-OH bending, shifting from about 1417 cm^{-1} to 1425 cm^{-1}. These shifts in peak positions and changes in the spectra indicate molecular interactions and alterations within the PGA-HA/PVA NFs structure induced by the addition of GMS [55]. The presence of GMS appears to influence the chemical environment, causing notable shifts and changes in the characteristic peaks associated with the functional groups of the polymer blend. This spectral analysis provides valuable insights into the molecular interactions and structural modifications occurring due to the incorporation of GMS within the PGA-HA/PVA NFs composite.

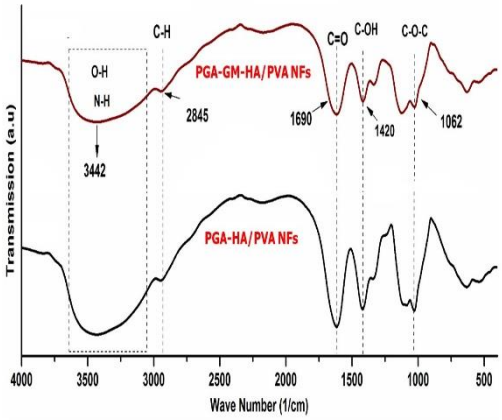

Figure 2: FTIR spectra of PGA-HA/PVA and PGA-GM-HA/PVA NFs

3.1.3. Mechanical properties

Figure 3 depicts the mechanical characteristics of both PGA-HA/PVA and PGA-GM-HA/PVA NFs. The tensile stress of the PGA-HA/PVA NFs, approximately 2.6 MPa, was nearly double that of the PGA-GM-HA/PVA NFs, around 1.7 MPa. However, the tensile strength of the PGA-HA/PVA NFs increased to 30%. The PGA-HA/PVA NFs displayed a notable enhancement in the stress-strain curve, signalizing reduced resistance to network deformation with increased gentamicin GMS content. This amelioration in the stress-strain proportion of the NFs is attributed to the structural presence of PGA-HA, which contributes as an extra crosslinking impact through the physical interaction among hyaluronan chains, PVA, and PGA chains[56]. The mechanical analysis of PGA-HA/PVA NFs with GMS suggests a distinctive impact on the material's tensile stress and strength. The presence of GMS seems to induce changes in the mechanical properties, potentially influencing the material's ability to withstand tensile forces and deformation[57].

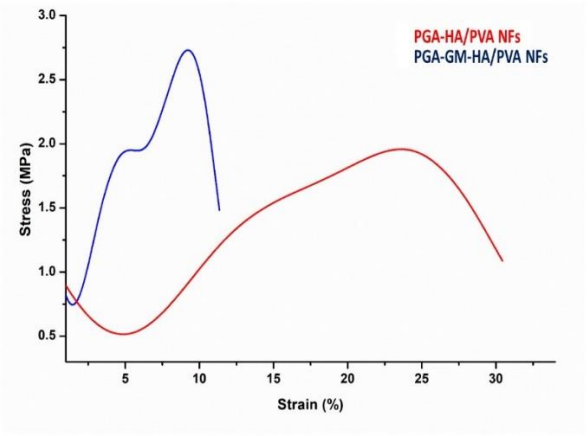

Figure 3: Tensile strength of PGA-HA/PVA and PGA-GM-HA/PVA NFs

3.1.4. The wettability of produced nanofibers

The observation of nanofiber wettability was conducted through contact angle measurements (refer to Fig. 4). The NFs produced, both PGA-HA/PVA and PGA-GM-HA/PVA NFs displayed water contact angles measuring 44° and 46°, respectively. Notably, PGA-GM-HA/PVA NFs exhibited the smallest contact angle, indicating the highest level of hydrophilicity. This outcome might be attributed to the increased presence of amine-functionalized hyaluronic acid within the biopolymers, which resulted in higher contact angle values[58].

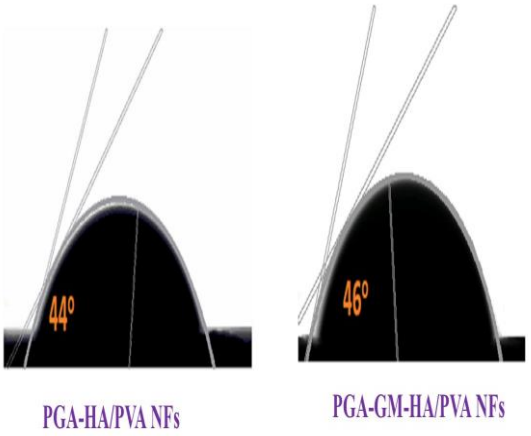

Figure 4: Wettability test by using a contact angle tester of PGA-HA/PVA and PGA-GM-HA/PVA NFs

3.2. HPLC method construction and optimization

The method was constructed to supply an optimized and simple procedure, with lowered cost and time of analysis. The method was developed to quantify GMS loaded in the fabricated PGA-GM-HA/PVA NFs. The validated method was considered as novel to quantify GMS using phenyl column. The suggested mobile phase is fundamentally comprising Acetonitrile and milliQ water (pH modified with formic acid to 3.0 ± 0.2 as ion paring reagent) in various ratios starting from 50: 50 to 10: 90 Acetonitrile and milliQ water acidified with formic acid solution. Using different columns involving C18 and C8, several issues were spotted like prolonged retention times, infrequent structural peak, and lack of reproducibility in the GMS peak. These issues

were settled by employing a phenyl column. The suggested procedure seemed to be modest and reproducible by employing a mobile phase involving Acetonitrile and milliQ water acidified with formic acid (20: 80 v/v).

3.3. Method optimization and validation

Linearity. The calibration curves for GMS was linear through the concentration limit of 1–9 mg% (Fig. 5). They demonstrated that the analytical procedures results are directly comparable. It was probable to connect between the GMS amount in the standard specimens with the peak area in the chromatograms. Linearity was estimated in triplicate, during the emergence and optical appraisal of the calibration curves by using an external standard solutions in the range among 1 and 9 mg% (Fig. 6 A& B shows 6 mg% HPLC chromatogram at 280nm and 212 nm respectively). R values exceeding 0.999 signalize a perfect linearity of the suggested method for GMS at 280, and 212, nm with r = 0.9992, and 0.9990 respectively.

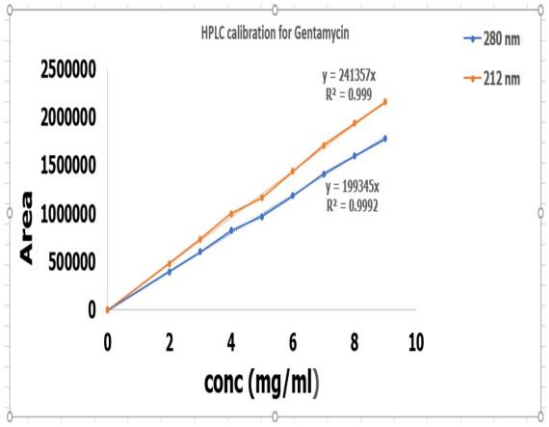

Figure 5: HPLC calibration for gentamicin at 280 and 212nm

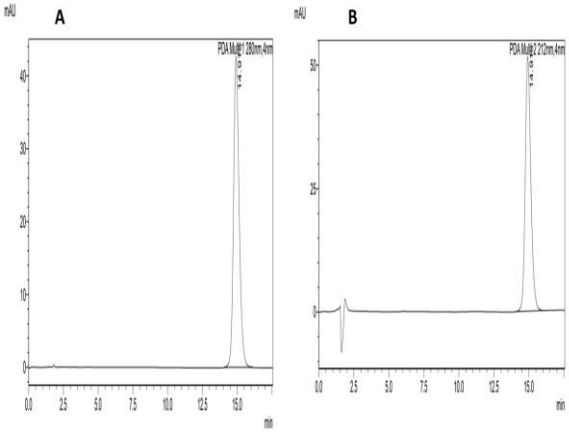

Figure 6: HPLC chromatograms for gentamicin standard solution (6 mg%) at 280 nm (A) and 212 nm (B)

3.4. Accuracy and precision of the developed method

Accuracy signalizes the connection among the acquired results and the true one. It may be resolved by enumerating the mean % recoveries for the GMS at various triple doses accompanied with the RSD [59]. The 3 standard concentrations (2, 6, and 9 mg%) were precisely made in triplicate, and every specimen was resolved by the newly developed analytical procedure on 3 non-sequential days (n = 3).

These concentrations were selected because they include the entire working scope. The overall mean recoveries were 98.95±1.39 % for GMS at 280 nm, and 98.97±1.39 % for GMS at 212 nm and displaying intense agreement among the theoretical and experimental amounts (Table 1).

The precision indicates the magnitude that the random errors can affect the efficiency of the newly developed process and could be presented at various scales[60]. In this study, the precision was estimated by testing 3 various standard concentration (2, 6, and 9 mg%) and exemplified by RSD.

Each standard concentration was made in triplicate, producing a whole of 9 specimens per day. Comparable to accuracy, the specimens employed to estimate the precision were evaluated throughout the linear working area. The intermediate precision, inter-day, was assessed by testing three various concentrations (2, 6 and 9 mg%) on 3 non-sequential days. The results are offered as ^{b} RSD (Table 2). The results elucidate perfect precision for the newly developed analytical method. RSD for repeatability at all standard concentration was 0.509937 for GMS at 280 nm, and 0.600357 for GMS at 212 nm (intraday n = 9) and 1.39 for GMS at 280 nm, and 212 nm (interday n = 3). The findings manifested preferable precision for the new analytical procedure.

3.5. Limit of detection and limit of quantification.

In this study, the LOD was detected to be 0.009 and 0.103 mg ml^{-1} for GMS at 280 nm and 212 nm respectively, while the LOQ was 0.028 and 0.34 mg ml^{-1} for GMS at 280 nm and 212 nm respectively. The method through the working area displayed higher precision, linearity, and accuracy [61, 62]. Table 3 offered the comparisons between the newly developed method and other methods validated by another systems employed for the analytical detection of GMS.

3.6. Determination of % EE (% entrapment efficiency)

The validated method was utilized for assessing the % EE of GMS in its novel developed NFs as presented in (Table 4). The GMS peak appear at their particular retention time. The results showed proper precision and accuracy as denoted by % EE±SD, and CV%.

3.7. *In vitro* Gentamicine release

The *in vitro* release of GMS showed a very slow release pattern from the fabricated NFs (5.932% release after 24 hrs.) then remained almost unchanged till the end of the experiment (5.98 % after 72 h) without significant initial burst effect (Fig. 7).On contrary to the free Gentamicin that completely diffused out of the dialysis after 4 h. (97.82 %). The results indicated that the manufactured NFs could successfully entrap GMS to avoid tissue toxicity related to exposure to high dose. In a previous study, a slow release of gentamicin from NF scaffold was extended for a longer duration of 18 days[14]. The slow release of GMS from the NFs might be attributed to the entrapment into the narrow lumen of the constructed NFs thus, facing difficulty to diffuse and reach easily to the open ends of the NFs[14]. Additionally, hyaluronic acid is negatively charged polymer and can easily form polyelectrolyte complexes with the negatively charged gentamicin as a delivery system thus contributing to its poor release[63].

Table 1: Accuracy and RSD for various standard concentrations of GMS evaluated at two different wavelengths

Nominal Concentration (mg %)	% Recovery[a] (inter-day n=3)		RSD (%) (n=9) [b]	
	280 nm	212 nm	280 nm	212 nm
2.00	99.41366	99.42982	0.289992	0.38787
6.00	97.42406	97.47957	3.036352	3.07305
9.00	100	100	0.858178	0.714692

[a] Presented as percentage of nominal tested concentration. [b] RSD.

Table 2: Intra and inter days precision for 3 various standard concentrations of GMS at two different wavelengths.

Nominal Concentration (mg%)	Day	Mean[a]		RSD [b] (%)	
		280 nm	212 nm	280 nm	212 nm
	Inter-day diversity (n = 3)				
2.00	1	1.989698	1.998031	0.262089	0.223268
6.00	1	5.966291	6.00	0.179199	1.748217
9.00	1	8.926481	8.964122	0.499852	0.219974
2.00	2	2.00	2.00	0.709087	0.460425
6.00	2	5.944473	5.966793	0.520148	1.121825
9.00	2	8.898402	8.935325	0.791949	0.453237
2.00	3	1.999844	1.998688	0.42796	0.188013
6.00	3	5.929758	5.935037	0.683143	0.684382
9.00	3	9.007971	9.024339	0.516016	0.303875
	Intra-day diversity (n=9 each level, 3 days)				
2.00	---	1.988273	1.988596	0.289992	0.38787
6.00	---	5.845444	5.854774	3.036352	3.07305
9.00	---	9.00	9.00	0.858178	0.714692

[a] average detected concentration (mg ml^{-1}). [b] RSD.

Taple 3: Comparison between Methods employed for the analytical detection of GMS.

Instrument	Sample form	Derivatizing agent	R^2	Sensitivity (µgmL^{-1})		Linear range (µgmL^{-1})	Ref.
				LOD	LOQ		
RP-HPLC	Pharmaceutical, blood, and urine	Hantzsch reagent	0.998	0.286	0.867	5 – 150	[64]
HPLC/UV	Pharmaceutical	O-Phthalaldehyde	1.0000	5	50	50 - 2000	[65]
HPLC–DAD	Pharmaceutical, blood, and urine	Hantzsch reagent	0.998	0.024	0.071	0.10–25.0	[66]
HPLC–DAD	Pharmaceutical	9-fluorenylmethyl chloroformate (FMOC-Cl)	0.999	0.01	0.032	0.05 - 5	[67]
ESI-MS	Pharmaceutical		0.9997	0.01	_	0.01-1	[26]
RP-HPLC-CAD	Pharmaceutical		0.99	1.58	3.7	1-200	[2]
HPLC/UV	Pharmaceutical	O-Phthalaldehyde	0.999	8	24	87 - 260	[68]
RP-HPLC-PDD	Pharmaceutical		0.999	9 at 280 nm 103 at 212 nm	28 at 280 nm 340 at 212 nm	10 - 90	This study

Table 4: %EE of gentamicin in the laboratory prepared nanofibers

Parameters	Gentamicin	
	280nm	212 nm
% EE±SD*	98.263 ± 2.564	98.550 ± 2.510
CV%	2.720	2.547

*Mean of % EE of three various constructed NFs

Table 5: Monitoring of wound reduction in the examined groups at different periods.

Treatment Period (Day)	Wound diameter (mm)		Wound area reduction (%)	
	Sterile gauze	PGA-GM-HA/PVA NFs	Sterile gauze	PGA-GM-HA/PVA NFs
Zero	15.59±0.17	15.47±0.13	0	0
3	15.21±0.07	13.65±0.18	4.8±1.39	22.14±2.28
7	13.76±0.19	9.605±0.25	21.89±2.88	61.43±1.37
10	10.79±0.18	4.55±0.28	52.09±1.78	91.32±1.16
14	5.3±0.26	0.67±0.58	88.45±1.01	99.73±0.24

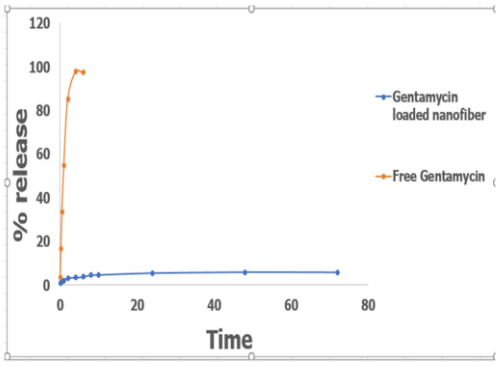

Figure 7: HPLC release of gentamicin

3.8. *In vivo* wound contraction

For observing the in vivo effectiveness of the constructed PGA-GM-HA/PVA NFs against full thickness wounded skin, the macroscopic images that allow the observation of the surface changes at the wounded region were periodically captured using a digital camera at particular time intervals for all animals. As stated in Fig. 8, PGA-GM-HA/PVA NFs treated rats offered the superior wound contraction rate as only 14 days were completely enough for perfect re-epithelialization on contrary to the rats applied sterile gauze. Observing the values of wound reduction % in the examined groups was displayed in Table 5. The rats applied the constructed PGA-GM-HA/PVA wound dressing NFs exhibited a considerable higher healing efficiency compared to those applied sterile gauze since after only 3 days, the size of the wounds of PGA-GM-HA/PVA NFs applied group retracted from about 15.47 to 13.65 mm, corresponding to a wound area reduction of 22.14% which exceed that of the sterile gauze group with a wound area reduction of 15.21% in the same period of time. Additionally, amelioration of the animals wounds applied PGA-GM-HA/PVA NFs were noticed over the experiment with a calculated contraction % reached more than 99% on day 14, while the registered contraction % in the wounds applied sterile gauze were only 88.45% on the same day. This healing interval of 14 days is deemed to be fully pleasurable compared to those treated wounds which was also carried out using the constructed (cHA/ZnO/CEO) nanofibers by other researchers, for a longer period of 17 days[37].

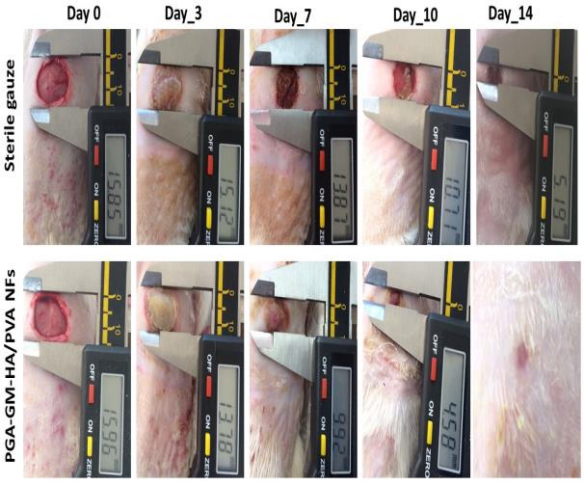

Figure 8: Images of in vivo full thickness excision wounds in tested animals

Fig. 9 distinctly explained the histopathological diversities among the normal and the wounded dorsal skin of the examined animals on day 14, either treated or untreated, stained employing the H&E technique and MTs. First of all, Fig. 9 A manifests the H&E stained healthy skin section with its primary features involving a dense epidermal layer enveloped by keratin, dermal layer involving hair follicles, blood vessels, sebaceous glands and connective tissue . On the 14th day of treatment, a fully significant distinction was noticed among the histopathological manifestations of both control or treated animals. The skin applied sterile gauze didn't retrieve the normal aspect and their skin exteriors were not entirely healed with less improved epidermal and dermal layers accompanied with the infiltration of diversified inflammatory cells and a slight engorged blood vessels and lack of hair follicles which distinctly demonstrates the healing impediment. On contrast, apparently healing skin tissue of the animals applied PGA-GM-HA/PVA NFs displayed well organized skin feature with entirely renewed epidermis and keratinocyte layer involving freshly created skin elements such as sebaceous glands, blood vessels, and hair follicles. Additionally, the epidermal layer was comprised with the tightly dense connective tissue which demonstrated the potentiality of the constructed nanofiber in accelerating wound healing with skin feature integrity similar to that noticed in normal skin tissue.

The histopathological variances among the normal and the treated injured skin of the examined animals were also tested employing MTS staining to show the intensity of deposition of blue collagen fiber and were stated in Fig. 9. The normal

skin stained MTS offered large, mature, well tight and uniform deposited collagen fibers architecture that provide a superior tensile strength for the skin tissue. However, compared to the normal skin, on day 14 the collagen fiber deposition of the injured skin applied sterile gauze were disorganized, loosely packed, and fragmented denoting a powerless tensile intensity. While the injured skin applied the PGA-GM-HA/PVA NFs displayed elevated mature collagen fibers depositions on the regenerated epidermis, symbolizing the normal skin manifestation. Therefore, the present outcomes inferred that the constructed PGA-GM-HA/PVA wound dressing NFs might enhance wound healing via promoting collagen deposition. Relatively perfect outcomes by PGA-GM-HA/PVA wound dressings NFs can be referred to the wound healing merits of the polymer matrix constituents encompassing HA known to amend the inflammation, angiogenesis, and cellular migration stages during healing[69] as well as PVA and PGA reported to participate in wound closure[70, 71]. Some studies favor the routine utilization of antibiotics in wound management owing to their preferable vascular and cellular propagation, thus hastening the cutaneous lesions closure, as well as being efficacious in diminishing infection[24, 72]. Several studies to date offer that topically applied gentamicin significantly ameliorate the healing quality and decrease the healing duration in infected wound[73, 74]. Other finding reported that topically applied gentamicin into open skin wound can improve wound closure via induction of new laminin 332, a protein required for epidermal-dermal adherence[75].

Despite very slow release pattern for PGA-GM-HA/PVA wound dressings NFs, It displayed preferable in vivo findings. This could be assigned to the naturally excreted degrading enzymes in the wound bed during the healing process involving proteases or proteinases. These proteinases support the elaboration of the wound bed and disintegrate the extracellular matrix components involving elastin and collagens preceding the complete wound occlusion and remodling[76]. Polymeric biodegradable materials could supply a valuable merits in wound care. They can degrade easily by the generated degrading enzymes and liberate their payload cargo[77]

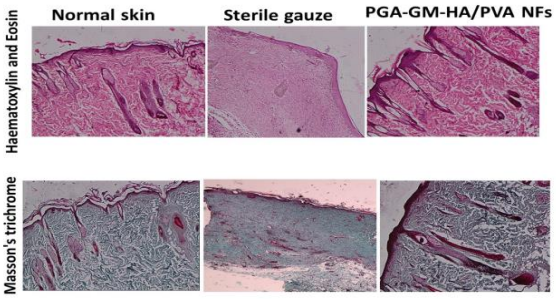

Figure 9: Histopathological analysis of normal and healed skin sections in tested animals on day 14 employing H&E (hematoxylin-eosin) staining, and MTS (Masson's trichrome stain) (Original magnification 100).

4. Conclusion

In conclusion, we have constructed electrospun nanofiber scaffolds based on the natural polymer HA and a biocompatible polymer PVA, and PGA incorporated GMS for wound healing applications. The constructed electrospun NFs exhibited a sustained GMS release to minimize the unfavorable side effects associated with burst release. The wider use of GMS in pharmaceutical formulations demands adequate analytical methods for their quantitative detection. The RF-HPLC method depicted in this work is the first rapid method, which can accurately quantify gentamicin by direct detection with no derivatization employing a Diode Array Detector. The method was successfully validated and has been demonstrated to have perfect linearity, accuracy, and precision. The SEM image confirmed the nanoscale diameter of the nanofiber (326 nm). More importantly, the in vivo wound healing performance manifested rapid tissue regeneration in terms of re-epithelization and reinforced collagen deposition on day 14. These results confirmed the superiority of the constructed nanofiber incorporated gentamicin as wound dressing material.

Conflicts of interest

"The authors declare that there is no conflict of interests regarding the publication of this article".

5. References

1. Hamza, K.H., et al., *Topically Applied Biopolymer-Based Tri-Layered Hierarchically Structured Nanofibrous Scaffold with a Self-Pumping Effect for Accelerated Full-Thickness Wound Healing in a Rat Model.* Pharmaceutics, 2023. **15**(5): p. 1518.
2. Joseph, A. and A. Rustum, *Development and validation of a RP-HPLC method for the determination of gentamicin sulfate and its related substances in a pharmaceutical cream using a short pentafluorophenyl column and a charged aerosol detector.* Journal of pharmaceutical and biomedical analysis, 2010. **51**(3): p. 521-531.
3. Umeki, S., *Anti-inflammatory action of gentamycin through inhibitory effect on neutrophil NADPH oxidase activity.* Comparative Biochemistry and Physiology Part B: Biochemistry and Molecular Biology, 1995. **110**(4): p. 817-821.
4. Anderson, R., *Erythromycin and roxithromycin potentiate human neutrophil locomotion in vitro by inhibition of leukoattractant-activated superoxide generation and autooxidation.* Journal of Infectious Diseases, 1989. **159**(5): p. 966-973.
5. Umeki, S., *Anti-inflammatory action of erythromycin: its inhibitory effect on neutrophil NADPH oxidase activity.* Chest, 1993. **104**(4): p. 1191-1193.
6. Abdelghany, S.M., et al., *Gentamicin-loaded nanoparticles show improved antimicrobial effects towards Pseudomonas aeruginosa infection.* International journal of nanomedicine, 2012: p. 4053-4063.
7. Batul, R., et al., *Polydopamine nanosphere with in-situ loaded gentamicin and its antimicrobial activity.* Molecules, 2020. **25**(9): p. 2090.
8. Soliman, G.M., et al., *Robust polymeric nanoparticles for the delivery of aminoglycoside antibiotics using carboxymethyldextran-b-poly (ethyleneglycols) lightly grafted with n-dodecyl groups.* Soft Matter, 2010. **6**(18): p. 4504-4514.
9. Ji, J., et al., *Preparation, characterization and in vitro release of chitosan nanoparticles loaded with gentamicin and salicylic acid.* Carbohydrate polymers, 2011. **85**(4): p. 803-808.
10. Abdelghany, S.M., et al., *Gentamicin-loaded nanoparticles show improved antimicrobial effects towards Pseudomonas aeruginosa*

infection. International journal of nanomedicine, 2012. **7**: p. 4053-4063.
11. Tamanna, T., et al., *Stability and controlled antibiotic release from thin films embedded with antibiotic loaded mesoporous silica nanoparticles.* RSC advances, 2015. **5**(130): p. 107839-107846.
12. Perni, S. and P. Prokopovich, *Continuous release of gentamicin from gold nanocarriers.* RSC advances, 2014. **4**(94): p. 51904-51910.
13. Dwivedi, C., et al., *Fabrication and assessment of gentamicin loaded electrospun nanofibrous scaffolds as a quick wound healing dressing material.* Current Nanoscience, 2015. **11**(2): p. 222-228.
14. Wali, A., et al., *In vivo wound healing performance of halloysite clay and gentamicin-incorporated cellulose ether-PVA electrospun nanofiber mats.* ACS Applied Bio Materials, 2019. **2**(10): p. 4324-4334.
15. Sahana, T. and P. Rekha, *Biopolymers: Applications in wound healing and skin tissue engineering.* Molecular biology reports, 2018. **45**: p. 2857-2867.
16. Sabra, S., et al., *Recent advances in electrospun nanofibers for some biomedical applications.* European Journal of Pharmaceutical Sciences, 2020. **144**: p. 105224.
17. Sharifi, F., et al., *Fiber based approaches as medicine delivery systems.* ACS Biomaterials Science & Engineering, 2016. **2**(9): p. 1411-1431.
18. Rezaei, A., A. Nasirpour, and M. Fathi, *Application of cellulosic nanofibers in food science using electrospinning and its potential risk.* Comprehensive Reviews in Food Science and Food Safety, 2015. **14**(3): p. 269-284.
19. Asghari, F., et al., *Biodegradable and biocompatible polymers for tissue engineering application: a review.* Artificial cells, nanomedicine, and biotechnology, 2017. **45**(2): p. 185-192.
20. El-Aassar, M., et al., *Controlled drug release from cross-linked κ-carrageenan/hyaluronic acid membranes.* International journal of biological macromolecules, 2015. **77**: p. 322-329.
21. Schanté, C.E., et al., *Chemical modifications of hyaluronic acid for the synthesis of derivatives for a broad range of biomedical applications.* Carbohydrate polymers, 2011. **85**(3): p. 469-489.
22. Kawano, Y., et al., *Wound healing promotion by hyaluronic acid: Effect of molecular weight on gene expression and in vivo wound closure.* Pharmaceuticals, 2021. **14**(4): p. 301.
23. Radhakrishnan, S., et al., *Fabrication of 3D printed antimicrobial polycaprolactone scaffolds for tissue engineering applications.* Materials Science and Engineering: C, 2021. **118**: p. 111525.
24. Altoé, L.S., et al., *Does antibiotic use accelerate or retard cutaneous repair? A systematic review in animal models.* PLoS One, 2019. **14**(10): p. e0223511.
25. Sofiqul, I. and P. Kumari, *Analytical Methods For The Determination Of Aminoglycosides Antibiotics By Chromatrographic Technique.* Int J Pharm Pharm Sci, 2020. **12**(4): p. 1-5.
26. Jariwala, F.B., et al., *Rapid determination of aminoglycosides in pharmaceutical preparations by electrospray ionization mass spectrometry.* Journal of Analytical Science and Technology, 2020. **11**(1): p. 1-11.
27. Caturla, M., E. Cusido, and D. Westerlund, *High-performance liquid chromatography method for the determination of aminoglycosides based on automated pre-column derivatization with o-phthalaldehyde.* Journal of Chromatography A, 1992. **593**(1-2): p. 69-72.
28. Stead, D.A., *Current methodologies for the analysis of aminoglycosides.* Journal of Chromatography B: Biomedical Sciences and Applications, 2000. **747**(1-2): p. 69-93.
29. Lu, C.-Y. and C.-H. Feng, *Micro-scale analysis of aminoglycoside antibiotics in human plasma by capillary liquid chromatography and nanospray tandem mass spectrometry with column switching.* Journal of Chromatography A, 2007. **1156**(1-2): p. 249-253.
30. Donegan, M., J.M. Nguyen, and M. Gilar, *Effect of ion-pairing reagent hydrophobicity on liquid chromatography and mass spectrometry analysis of oligonucleotides.* Journal of Chromatography a, 2022. **1666**: p. 462860.
31. Chakraborty, A.B. and S.J. Berger, *Optimization of reversed-phase peptide liquid chromatography ultraviolet mass spectrometry analyses using an automated blending methodology.* Journal of biomolecular techniques: JBT, 2005. **16**(4): p. 327–335.
32. Boot, W., et al., *A hyaluronic acid hydrogel loaded with gentamicin and vancomycin successfully eradicates chronic methicillin-resistant Staphylococcus aureus orthopedic infection in a sheep model.* Antimicrobial Agents and Chemotherapy, 2021. **65**(4): p. 1-16.
33. Ter Boo, G.-J.A., et al., *Injectable gentamicin-loaded thermo-responsive hyaluronic acid derivative prevents infection in a rabbit model.* Acta biomaterialia, 2016. **43**: p. 185-194.
34. Michalska-Sionkowska, M., et al., *Antimicrobial activity of new materials based on the blends of collagen/chitosan/hyaluronic acid with gentamicin sulfate addition.* Materials Science and Engineering: C, 2018. **86**: p. 103-108.
35. AlSalem, H.S. and A.A.H. Bukhari, *Biodegradable wound dressing-based collagen/hyaluronic acid loaded antibacterial agents for wound healing application.* International Journal of Biological Macromolecules, 2023. **242**: p. 124700.
36. El-Shanshory, A.A., et al., *Metronidazole topically immobilized electrospun nanofibrous scaffold: Novel secondary intention wound healing accelerator.* Polymers, 2022. **14**(3): p. 454.
37. Mohamed, R., et al., *Antibiotic-free combinational hyaluronic acid blend nanofibers for wound healing enhancement.* International journal of biological macromolecules, 2021. **167**: p. 1552-1563.
38. ICH Q2B, M., *Validation of analytical procedures: Methodology.* Guidance for Industry: Q2B Validation of Analytical Procedures: Methodology, 1996.
39. Agwa, M., et al., *Development and validation of a robust analytical method to quantify both*

etoposide and prodigiosin in polymeric nanoparticles by reverse-phase high-performance liquid chromatography. Analytical Methods, 2018. **10**(19): p. 2272-2280.
40. Aboras, S.I., et al., *HPLC with fluorescence detection for the bioanalysis and pharmacokinetic study of Doxorubicin and Prodigiosin loaded on eco-friendly casein nanomicelles in rat plasma.* Journal of Chromatography B, 2021. **1187**: p. 123043.
41. Peters, F.T., O.H. Drummer, and F. Musshoff, *Validation of new methods.* Forensic science international, 2007. **165**(2-3): p. 216-224.
42. Sarmento, B., et al., *Development and validation of a rapid reversed-phase HPLC method for the determination of insulin from nanoparticulate systems.* Biomedical Chromatography, 2006. **20**(9): p. 898-903.
43. Singh, J., *International conference on harmonization of technical requirements for registration of pharmaceuticals for human use.* Journal of Pharmacology and Pharmacotherapeutics, 2015. **6**(3): p. 185-187.
44. Agwa, M.M., et al., *Self-assembled lactoferrin-conjugated linoleic acid micelles as an orally active targeted nanoplatform for Alzheimer's disease.* International Journal of Biological Macromolecules, 2020. **162**: p. 246-261.
45. Agwa, M.M., et al., *Vitamin D3/phospholipid complex decorated caseinate nanomicelles for targeted delivery of synergistic combination therapy in breast cancer.* International Journal of Pharmaceutics, 2021. **607**: p. 120965.
46. Agwa, M.M., et al., *Potential of frankincense essential oil-loaded whey protein nanoparticles embedded in frankincense resin as a wound healing film based on green technology.* Journal of Drug Delivery Science and Technology, 2022. **71**: p. 103291.
47. Fayez, M.S., et al., *Topically applied bacteriophage to control multi-drug resistant Klebsiella pneumoniae infected wound in a rat model.* Antibiotics, 2021. **10**(9): p. 1048.
48. Abdelsattar, A.S., et al., *Enhancement of wound healing via topical application of natural products: in vitro and in vivo evaluations.* Arabian Journal of Chemistry, 2022. **15**(6): p. 103869.
49. Rezk, N., et al., *Bacteriophage as a potential therapy to control antibiotic-resistant Pseudomonas aeruginosa infection through topical application onto a full-thickness wound in a rat model.* Journal of Genetic Engineering and Biotechnology, 2022. **20**(1): p. 1-16.
50. El-Aassar, M., et al., *Wound healing of nanofiber comprising Polygalacturonic/Hyaluronic acid embedded silver nanoparticles: In-vitro and in-vivo studies.* Carbohydrate polymers, 2020. **238**: p. 116175.
51. Tamer, T., et al., *Wound dressing membranes based on immobilized Anisaldehyde onto (chitosan-GA-gelatin) copolymer: In-vitro and in-vivo evaluations.* International Journal of Biological Macromolecules, 2022. **211**: p. 94-106.
52. Shalaby, M., et al., *Fish scale collagen preparation, characterization and its application in wound healing.* Journal of Polymers and the Environment, 2020. **28**: p. 166-178.
53. Abdel-Mohsen, A., et al., *Electrospinning of hyaluronan/polyvinyl alcohol in presence of in-situ silver nanoparticles: Preparation and characterization.* International journal of biological macromolecules, 2019. **139**: p. 730-739.
54. Séon-Lutz, M., et al., *Electrospinning in water and in situ crosslinking of hyaluronic acid/cyclodextrin nanofibers: Towards wound dressing with controlled drug release.* Carbohydrate polymers, 2019. **207**: p. 276-287.
55. Liu, Y., et al., *Simultaneous enhancement of strength and toughness of PLA induced by miscibility variation with PVA.* Polymers, 2018. **10**(10): p. 1178.
56. Chen, J., et al., *Biomechanics of oral mucosa.* Journal of the Royal Society Interface, 2015. **12**(109): p. 20150325.
57. Kim, I.-Y., et al., *Preparation of semi-interpenetrating polymer networks composed of chitosan and poloxamer.* International journal of biological macromolecules, 2006. **38**(1): p. 51-58.
58. Hassan, C.M., P. Trakampan, and N.A. Peppas, *Water solubility characteristics of poly (vinyl alcohol) and gels prepared by freezing/thawing processes.* Water soluble polymers: solutions properties and applications, 2002: p. 31-40.
59. Sarkar, M., S. Khandavilli, and R. Panchagnula, *Development and validation of RP-HPLC and ultraviolet spectrophotometric methods of analysis for the quantitative estimation of antiretroviral drugs in pharmaceutical dosage forms.* Journal of Chromatography B, 2006. **830**(2): p. 349-354.
60. Argekar, A. and J. Sawant, *Determination of cisapride in pharmaceutical dosage forms by reversed-phase liquid chromatography.* Journal of Pharmaceutical and Biomedical Analysis, 1999. **21**(1): p. 221-226.
61. das Neves, J., et al., *Development and validation of a rapid reversed-phase HPLC method for the determination of the non-nucleoside reverse transcriptase inhibitor dapivirine from polymeric nanoparticles.* Journal of pharmaceutical and biomedical analysis, 2010. **52**(2): p. 167-172.
62. Taverniers, I., M. De Loose, and E. Van Bockstaele, *Trends in quality in the analytical laboratory. II. Analytical method validation and quality assurance.* TrAC Trends in Analytical Chemistry, 2004. **23**(8): p. 535-552.
63. ter Boo, G.J.A., et al., *Hyaluronic acid derivatives and its polyelectrolyte complexes with gentamicin as a delivery system for antibiotics.* Polymers for advanced technologies, 2017. **28**(10): p. 1325-1333.
64. Maheshwari, M., et al., *Validated RP-HPLC method development for gentamicin microanalysis in pharmaceutical dosage forms, urine and blood.* Pharmaceutical Chemistry Journal, 2021. **55**(5): p. 524-530.
65. Kuehl, P., et al., *Development and validation of an HPLC assay for dual detection of gentamicin*

sulfate and leucine from a novel dry powder for inhalation. J. Anal. Bioanal. Tech, 2012. **3**: p. 1-4.
66. Maheshwari, M.L., et al., *A rapid HPLC–DAD method for quantification of amikacin in pharmaceuticals and biological samples using pre-column derivatization with Hantzsch reagent.* Journal of the Iranian Chemical Society, 2021. **18**: p. 611-620.
67. Sionkowska, A., B. Kaczmarek, and R. Gadzala-Kopciuch, *Gentamicin release from chitosan and collagen composites.* Journal of Drug Delivery Science and Technology, 2016. **35**: p. 353-359.
68. Fiolet, A.-S., et al., *Long-term stability of gentamicin sulfate-ethylenediaminetetraacetic acid disodium salt (EDTA-Na2) solution for catheter locks.* Journal of Pharmaceutical Analysis, 2018. **8**(6): p. 386-393.
69. Muto, J., et al., *Emerging evidence for the essential role of hyaluronan in cutaneous biology.* Journal of dermatological science, 2019. **94**(1): p. 190-195.
70. Rieger, K.A. and J.D. Schiffman, *Electrospinning an essential oil: Cinnamaldehyde enhances the antimicrobial efficacy of chitosan/poly (ethylene oxide) nanofibers.* Carbohydrate polymers, 2014. **113**: p. 561-568.
71. Kim, M.-S., et al., *Antimicrobial hydrogels based on PVA and diphlorethohydroxycarmalol (DPHC) derived from brown alga Ishige okamurae: An in vitro and in vivo study for wound dressing application.* Materials Science and Engineering: C, 2020. **107**: p. 110352.
72. Dreifke, M.B., A.A. Jayasuriya, and A.C. Jayasuriya, *Current wound healing procedures and potential care.* Materials Science and Engineering: C, 2015. **48**: p. 651-662.
73. Gao, Y., et al., *A gentamicin-thioctic acid multifunctional hydrogel for accelerating infected wound healing.* Journal of Materials Chemistry B, 2022. **10**(13): p. 2171-2182.
74. Wang, P., et al., *The efficacy of topical gentamycin application on prophylaxis and treatment of wound infection: a systematic review and meta-analysis.* International Journal of Clinical Practice, 2019. **73**(5): p. e13334.
75. Kwong, A., et al., *Gentamicin induces laminin 332 and improves wound healing in junctional epidermolysis bullosa patients with nonsense mutations.* Molecular Therapy, 2020. **28**(5): p. 1327-1338.
76. Cutting, K.F., *Wound exudate: composition and functions.* British journal of community nursing, 2003. **8**(Sup3): p. S4-S9.
77. Gosai, H., et al., *Role of Biodegradable Polymer-Based Biomaterials in Advanced Wound Care.* Wound Healing Research: Current Trends and Future Directions, 2021: p. 599-620.